Modern Physics Letters B, Vol. 23, No. 23 (2009) 2807–2818

World Scientific
www.worldscientific.com

COMPARISON OF TWO-VALLEY HYDRODYNAMIC MODEL IN BULK SiC AND ZnO MATERIALS

H. ARABSHAHI*, REZAEE ROKN-ABADI and S. GOLAFROZ

Department of Physics, Ferdowsi University of Mashhad,
P. O. Box 91775-1436, Mashhad, Iran
** arabshahi@um.ac.ir*

Received 7 December 2008
Revised 18 March 2009

This report reviews the feasibility of two-dimensional hydrodynamic models in bulk SiC and ZnO semiconductor materials. Although the single-gas hydrodynamic model is superior to the drift-diffusion or energy balance model, it is desirable to direct the efforts of future research in the direction of multi-valley hydrodynamic models. The hydrodynamic model is able to describe inertia effects which play an increasing role in different fields of micro and optoelectronics where simplified charge transport models like the drift-diffusion model and the energy balance model are no longer applicable. Results of extensive numerical simulations are shown for SiC and ZnO materials, which are in fair agreement with other theoretical or experimental methods.

Keywords: Hydrodynamic; drift-diffusion; multi-valley; optoelectronics

1. Introduction

Wide-bandgap semiconductors, such as SiC and ZnO, have come to the forefront in the past decade because of an increasing need for short-wavelength photonic devices and high-power, high-frequency electronic devices, and because of breakthroughs in high-quality growth of these materials. SiC and ZnO semiconductor materials have not received much attention, probably because these materials have been perceived as being useful only in their polycrystalline form. Indeed, polycrystalline SiC and ZnO have found numerous applications in diverse areas such as facial powders, piezoelectric transducers, varistors, phosphors, and transparent conducting films. Recently, however, large area bulk growth has been achieved,[1] and, furthermore, several epitaxial methods have produced excellent materials.[2–6]

Semiconductor device modeling includes a wide range of areas in solid state physics, applied and computational mathematics. Transport of carriers in semiconductors under an applied electric field was first explained as a combination of drift due to the field, and diffusion due to concentration gradients. In the presence of high fields that change rapidly over small distances, the drift-diffusion equations, however, lose thier validity and non-local and hot-carrier effects begin to dominate device performance. In effect, apart from carrier density and velocity, carrier

energy (or equivalently, temperature) needs to be considered because the carriers are not in thermal equlibrium with the lattice. In SiC and ZnO materials which are used for high-speed device design,[7,8] inertia effects play an important role since the impulse and energy relaxation times of the electron gas are close to the picosecond range. The most elaborate and practicable approach for the description of charge transport in semiconductors used for device simulation would be the Monte Carlo method.[9−11] The advantage of this technique is a complete picture of carrier dynamics with reference to microscopic material parameters, e.g. effective masses and scattering parameters. But the method is still considered to be very time consuming and hence not economical to be used by device designers.

Besides the simplest concept which is the traditional drift-diffusion model, there is a much more rigorous approach to the problem, namely the so-called hydrodynamic model. The hydrodynamic model we are interested in is an extension of the drift diffusion equations. It consists of a set of Euler equations with certain source terms and a Poisson equation for the electrical potential.[12−15] This model is capable of capturing some important features of semiconductor devices which are not accounted for in the classical drift-diffusion model.

This paper is organized as follows. In Sec. 2, we give a short definition of the hydrodynamic model for wurtzite SiC in comparison with ZnO structure. It is emphasized that a analysis of the physical features of the charge carrier transport models is the basis for a clear understanding of their limits of applicability. In Sec. 3, the two-valley hydrodynamic model in SiC and ZnO crystal structures are interpreted.

2. Model and Basic Equations

Single-gas hydrodynamic equations have been carried out to simulate the electron transport properties in bulk SiC and ZnO materials. We have used an analytical band structure model consisting of two non-parabolic ellipsoidal valleys (Γ and U valleys in wurtzite structure). The equations for each valley are, however, coupled through collision terms since electrons can scatter between two different valleys. The corresponding relaxation rates may be of the order of a picosecond and are therefore relatively large. This is why we have to implement at least a two-valley hydrodynamic model. Reliable extensive two-valley simulations have been performed only for the one-dimensional case so far due to the large amount of equations and parameters involved in such a model. The hydrodynamic model equations consist of the continuity equation

$$\frac{\partial n}{\partial t} + \boldsymbol{\nabla} \cdot \mathbf{j} = 0\,. \tag{1}$$

For unipolar devices it is possible to neglect charge carrier generation and recombination term so the momentum balance equations is given by

$$\frac{\partial \mathbf{p}}{\partial t} + (\nabla \mathbf{p})v + (p\boldsymbol{\nabla})v = -en\mathbf{E} - \boldsymbol{\nabla}(nkT) - \frac{\mathbf{p}}{\tau_p}\,, \tag{2}$$

or alternatively (only for the x-component)

$$\frac{\partial[m^*(\epsilon')n\mathbf{v}_x]}{\partial t} + \boldsymbol{\nabla}[m^*(\epsilon')n\mathbf{v}_x v] = -qn\mathbf{E}_x - \frac{\partial(nkT)}{\partial x} - \frac{m^*(\epsilon')n\mathbf{v}_x}{\tau_p(\epsilon')}\,, \tag{3}$$

and the energy balance equation is

$$\frac{\partial\epsilon}{\partial t} + \boldsymbol{\nabla}(v\epsilon) = -qnv\mathbf{E} - \boldsymbol{\nabla}(nkTv) - \boldsymbol{\nabla}(-k\boldsymbol{\nabla}T) - \frac{\epsilon - \frac{3}{2}nkT_L}{\tau_\epsilon(\epsilon')}\,, \tag{4}$$

where n, ϵ ($\epsilon' = \epsilon/n$), and v are the electron density, the electron energy density (average electron energy) and the electron drift velocity, respectively. $\mathbf{v}_x$ is the x-component of the electron drift velocity and $\mathbf{p} = m^*n\mathbf{v}$ is the momentum density. Corresponding equations are valid for the y and z components. T is the electron temperature and $\epsilon_0' = 3/2kT_L$ is the average thermal equilibrium energy of electrons, where T_L is the lattice temperature. The electronic current density $\mathbf{j}$ inside the active device is $\mathbf{j} = -ne\mathbf{v}$, so the total current density is

$$\mathbf{j}_t = -ne\mathbf{v} + \epsilon_0\epsilon_r\frac{\partial\mathbf{E}}{\partial t}\,. \tag{5}$$

The momentum relaxation time $\tau_p(\epsilon')$ is related to the mobility of the electrons via $\mu(\epsilon') = e/m^*(\epsilon')\tau_p(\epsilon')$, and the energy relaxation time $\tau_\epsilon(\epsilon')$ describes the exchange of energy between the heated electron gas and the lattice. τ_p and τ_ϵ and the effective electron mass m^* are assumed to be functions of the mean electron energy.

The hydrodynamic equations, together with Poisson's equation

$$\Delta\phi = -\boldsymbol{\nabla}E = -\frac{e}{\epsilon_0\epsilon_r}(N_d^+ - n) \tag{6}$$

form a complete set of equations that can be used to solve for the electron density, velocity, energy and electric field for given boundary conditions. A closing relation for the mean electron energy ϵ', the electron temperatute T and velocity $\mathbf{v}$ is

$$\epsilon' = \frac{1}{2}m^*(\epsilon')v^2 + \frac{3}{2}kT + \beta_U(\epsilon')\Delta E_{\Gamma U}\,. \tag{7}$$

The last term in Eq. (7) accounts for the fact that a minimum energy of about $\Delta E_{\Gamma U} = 1.5$ eV is necessary to excite an electron from central Γ-valley to the nearest upper valley in both SiC and ZnO structures. β_U is the relative fraction of electrons in the U-valley for the stationary homogeneous case. The term $\beta_U(\epsilon')\Delta E_{\Gamma U}$ is often neglected, but this may lead to an overestimation of the electron temperature of more than 1000 K at high energies.

Due to using a single-gas approximation for the hydrodynamic model, the electron temperature has been calculated from the total electron energy and electron drift velocity. The transition from the two-gas model to the single-gas approximation has to be done carefully, therefore here a short discussion of the problem has

been presented. The effect of the non-parabolicity of the energy band took into account the Kane model,[16]

$$\gamma(k) = E(\mathbf{k})[1 + \alpha_i E(\mathbf{k})] = \frac{\hbar^2}{2}\left[\frac{k_x^2 + k_y^2}{m_\perp^*} + \frac{k_z^2}{m_\parallel^*}\right], \tag{8}$$

where $m_\perp^*$ and $m_\parallel^*$ are the transverse and longitudinal effective masses at the band edge and α_i is the non-parabolicity coefficient of the ith valley. The electron velocity in a non-parabolic valley is given by

$$v = \frac{1}{\hbar}\frac{\partial E_k}{\partial k} = \frac{\hbar k}{m^*}\frac{1}{\sqrt{1 + 4\alpha\gamma(k)}}, \tag{9}$$

which implies that crystal velocity v and crystal momentum $p = \hbar k$ are related by

$$p = m^* v\sqrt{1 + 4\alpha\gamma(k)}\,. \tag{10}$$

In the single particle two-valley model, the probability β_Γ that an electron resides in the central Γ-valley is a function of the applied constant homogeneous electric field or a function of the mean electron energy. The probability of finding the electron in an upper U-valley is then $\beta_U = 1 - \beta_\Gamma$. The values of the average electron velocities in the different valleys can be obtained, so it is reasonable to define the average electron velocity by

$$v = \beta_\Gamma v_\Gamma + \beta_U v_U\,. \tag{11}$$

The average electron momentum p is given by

$$p = m^* v = m_\Gamma \beta_\Gamma v_\Gamma + m_U \beta_U v_U\,. \tag{12}$$

Thus the electron mass which must be used in the hydrodynamic model in order to relate average electron velocity and electron momentum is calculated by

$$m^* = \frac{m_\Gamma \beta_\Gamma v_\Gamma + m_U \beta_U v_U}{\beta_\Gamma v_\Gamma + \beta_U v_U}\,. \tag{13}$$

Important parameters used throughout the calculations are listed in Tables 1 and 2. Band edge energies, electron effective masses and non-parabolicities are derived from empirical pseudopotential calculations.[17–20] In our simulated model time discretization is used for all the hydrodynamic equations by forward Euler differencing method. The discretization is always written down only for the x-component of vectorial quantities in the sequel, since the corresponding expressions for y-components are easy to drive. The simplest method for assigning charged particles to cells is the nearest-grid-point scheme in which the total charge found in a cell is assigned to the midpoint of that cell. After each sampling Poisson's equation is solved and the electric field is updated. Poisson's equation is solved by a combined fast Fourier transform[21,22] and Buneman cyclic reduction method[23,24] developed by Walmsley and Abram.[25] This calculational scheme is integrated with a capacity

Table 1. Important band structure parameters used for SiC and ZnO materials.

	Valley	E_{gap} (eV)	$^{\dagger}m_{\parallel}$	$^{\dagger}m_{\perp}$	Nonparabolicity (eV^{-1})
SiC	Γ	3.2	0.22	0.45	0.323
	U	5.3	0.9	0.7	0.6
ZnO	Γ	3.43	0.27	0.4	0.66
	U	5.6	0.75	0.9	0.05

†, $\parallel$ denotes parallel to the (0001)c-axis and $\perp$ perpendicular to (0001)c-axis.

Table 2. Material parameter selections for SiC and ZnO.

	SiC	ZnO
Density ρ (kgm^{-3})	3200	6500
Sound velocity v_s (ms^{-1})	1373	6400
Low-frequency dielectric constant ϵ_s	9.7	8.2
High-frequency dielectric constant ϵ_∞	6.5	3.7
Acoustic deformation potential D (eV)	15	15
Polar optical phonon energy $\hbar\omega_{po}$ (eV)	0.012	0.072
Energy band gap (eV)	3.2	3.43

matrix approach[26] that facilitates the use of individual rectangular regions to form more complicated structures. Poisson's equation is expressed in discrete form as a set of three-point finite difference equations.

After setting all the material and device parameters, the simulation is started in a state of charge neutrality everywhere in the device. The simulated particles are distributed appropriately among all the mesh cells to achieve the required neutrality. In the two-dimensional device models used here there is no variation of electron density or electric field normal to the x–y plane and scalar quantities at a timestep like electron density $n^t_{i,j}$, energy $\epsilon^t_{i,j}$, temperature $T^t_{i,j}$ and potential $\phi^t_{i,j}$, are located at the center of the cells, whereas vectorial quantities like the electric field components $E^t_{x;i+\frac{1}{2},j}$, $E^t_{y;i+j+\frac{1}{2}}$ or the velocity components $v^t_{x;i+\frac{1}{2},j}$, $v^t_{y;i+j+\frac{1}{2}}$ are always calculated first at midpoint between the scalar quantities. For example, we can define for electric field the intermediate value as

$$E_{x;i,j} = \frac{1}{2}(E_{x;i-\frac{1}{2},j} + E_{x;i+\frac{1}{2},j})\,. \tag{14}$$

The fundamental quantities are calculated using boundary conditions at each timestep. For example, the momentum balance equation is discretized in the

following form:

$$\begin{aligned}\frac{p^{t+1}_{x;i+\frac{1}{2},j}-p^{t}_{x;i+\frac{1}{2},j}}{\Delta t} &= -qn^{t}_{i+\frac{1}{2},j}E^{t}_{x;i+\frac{1}{2},j}-\frac{k}{\Delta x}(n^{t}_{i+1,j}T^{t}_{i+1,j}-n^{t}_{i,j}T^{t}_{i,j})/n^{t}_{i+\frac{1}{2},j}\\ &-(p^{t}_{x;i+\frac{1}{2},j}v_{x;i+\frac{1}{2},j}-p^{t}_{x;i-\frac{1}{2},j}v_{x;i-\frac{1}{2},j})/\Delta x\\ &-(p^{t}_{x;i+\frac{1}{2},j}v_{y;i,j+\frac{1}{2},j}-p^{t}_{x;i+\frac{1}{2},j-1}v_{y;i,j-\frac{1}{2}}/\Delta y\\ &-p^{t}_{x;i+\frac{1}{2},j}/\tau^{t}_{p;i+\frac{1}{2},j}\,, \end{aligned}\tag{15}$$

where $p_{x;i+\frac{1}{2},j}\geq 0$ and $p_{y;i,j+\frac{1}{2}}\geq 0$ and the same discretization are used in the y-direction of the electron velocity as well. From the momentum density we can obtain the new particle current density by

$$j^{t+1}_{x;i+\frac{1}{2},j}=p^{t+1}_{x;i+\frac{1}{2},j}/m^{*}_{i+\frac{1}{2},j}\,,\tag{16}$$

and the momentum density at (i,j) is extrapolated from neighboring points in the direction of the electron flow x-component

$$\begin{aligned}p^{t+1}_{x;i,j}&=\frac{3}{2}p^{t+1}_{x;i-\frac{1}{2},j}-\frac{1}{2}p^{t+1}_{x;i-\frac{3}{2},j}\ :\ p^{t+1}_{x;i+\frac{1}{2},j}\geq 0\,,\\ p^{t+1}_{x;i,j}&=\frac{3}{2}p^{t+1}_{x;i+\frac{1}{2},j}-\frac{1}{2}p^{t+1}_{x;i+\frac{3}{2},j}\ :\ p^{t+1}_{x;i+\frac{1}{2},j}\leq 0\,,\end{aligned}\tag{17}$$

and finally we have

$$v^{t+1}_{x;i,j}=p^{t+1}_{x;i,j}/n^{t}_{i,j}/m^{*t}_{i,j}\,,\tag{18}$$

$$v^{t+1}_{x;i+\frac{1}{2},j}=j^{t+1}_{x;i+\frac{1}{2},j}/n^{t}_{i+\frac{1}{2},j}/m^{*t}_{i+\frac{1}{2},j}\,.\tag{19}$$

The electron temperature is related to the energy density by the relation $\epsilon^{t}_{i,j}=\frac{3}{2}n^{t}_{i,j}kT^{t}_{i,j}+\frac{1}{2}m^{*}_{i,j}n^{t}_{i,j}(v^{2t}_{x;i,j}+v^{2t}_{y;i,j})+\beta^{t}_{U;i,j}\Delta E_{\Gamma U}$ and is assumed to be the dependent variable. The upwind discretization of the energy balance equation is given by

$$\begin{aligned}\frac{\epsilon^{t+1}_{i,j}-\epsilon^{t}_{i,j}}{\Delta t} &= -en^{t}_{i,j}(v^{t+1}_{x;i,j}E^{t}_{x;i,j}+v^{t+1}_{y;i,j}E^{t}_{y;i,j})-\frac{\epsilon^{t}_{i,j}-\frac{3}{2}n^{t}_{i,j}kT_{L}}{\tau^{t}_{\epsilon;i,j}}\\ &-(j^{t}_{x;e,i+\frac{1}{2},j}-j^{t}_{x;e,i-\frac{1}{2},j})/\Delta x-(j^{t}_{x;p,i+\frac{1}{2},j}-j^{t}_{x;p,i,i-\frac{1}{2},j})/\Delta x\\ &-(j^{t}_{x;h,i,j+\frac{1}{2}}-j^{t}_{x;h,i-\frac{1}{2},j})/\Delta x-(j^{t}_{y;e,i,j+\frac{1}{2},j}-j^{t}_{y;e,i,j-\frac{1}{2}})/\Delta y\\ &-(j^{t}_{y;p,i,j+\frac{1}{2}}-j^{t}_{y;p,i,j-\frac{1}{2}})/\Delta y-(j^{t}_{y;h,i,j+\frac{1}{2}}-j^{t}_{y;h,i,j-\frac{1}{2}})/\Delta y\,,\end{aligned}\tag{20}$$

where the energy current density is defined as

$$j^{t}_{x;e,i+\frac{1}{2},j}=v^{t+1}_{x;i+\frac{1}{2},j}\epsilon^{t}_{i+\frac{1}{2},j}\,,\tag{21}$$

$$j^{t}_{x;p,i+\frac{1}{2},j}=kj^{t+1}_{x;i+\frac{1}{2},j}T^{t}_{i+\frac{1}{2},j}\,,\tag{22}$$

and

$$j^t_{x;h,i+\frac{1}{2},j} = k^t_{i+\frac{1}{2},j}(T^t_{i+1,j} - T^t_{i,j})/\Delta x\,. \tag{23}$$

Using the calculated mean electron energy, the other electron transport parameters are also updated. Also, using the particle current density $j = nv$, the current continuity equation is discretized in a conservative way as

$$\frac{n^{t+1}_{i,j} - n^t_{i,j}}{\Delta t} = -(j^t_{x;,i+\frac{1}{2},j} - j^t_{x;i-\frac{1}{2},j})/\Delta x - (j^t_{y;,i+j+\frac{1}{2}} - j^t_{y;i,j-\frac{1}{2}})/\Delta y\,. \tag{24}$$

The particles that leave cell (i, j) in the x-direction enter cell $(i + 1, j)$ and analogously for the y-direction.

3. Simulation Results

Figure 1 shows the average energy of an electron in a constant homogeneous electric field for SiC in comparison to the ZnO structure. For each data point, the electron was scattered one million times (including so-called self-scattering), therefore the resulting curve is already quite smooth. It can be seen that initially, kinetic energy increases with the electric field, due to the large proportion of electrons in the low mass central Γ valley of both crystal structures. However, as the field increases, the electrons transfer to higher valley with higher mass and increased scattering which causes a substantial reduction in the rate of increase of average kinetic energy. The detailed differences in the behavior of the average electron energy with field for the two crystal structures is simply due to the different band structure features.

In order to complete the set of data which is necessary for hydrodynamic simulation, the electron velocity-field characteristics and energy relaxtion times are

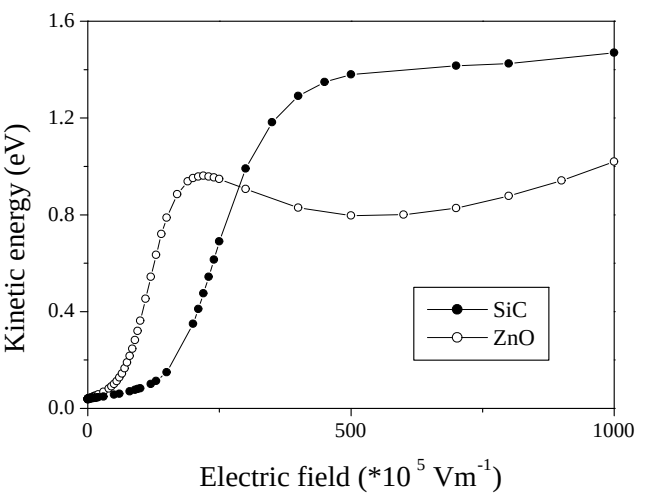

Fig. 1. Total average electron kinetic energy as a function of applied electric field in bulk SiC and ZnO at room temperature with $N_d = 10^{17}$ cm^{-3}.

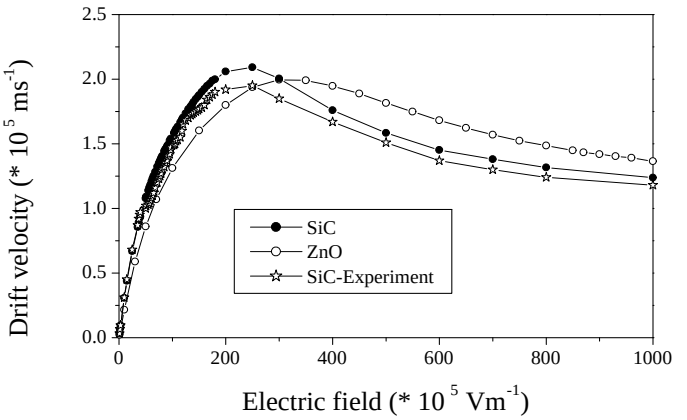

Fig. 2. Comparison of calculated steady state electron drift velocity in bulk SiC and ZnO with experiment results for SiC at room temperature with $N_d = 10^{17}\text{cm}^{-3}$.[27,28]

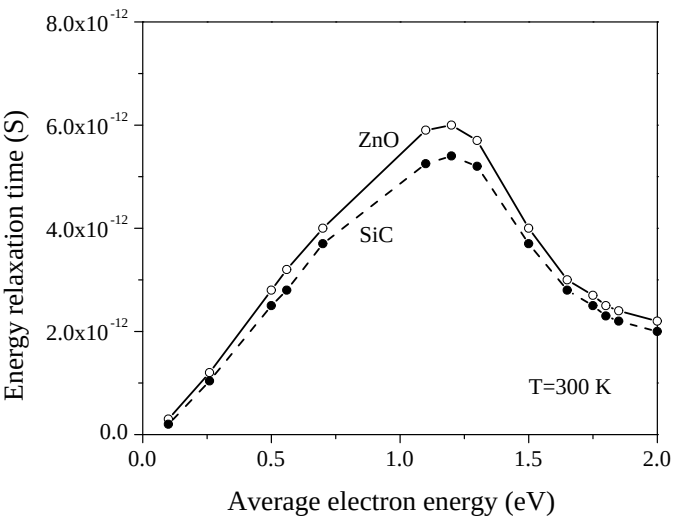

Fig. 3. Energy relaxation times for SiC and ZnO at room temperature with $N_d = 10^{17}$ cm^{-3}.

depicted in Figs. 2 and 3 for both SiC and ZnO structures. The characteristic shape of the velocity curve can be explained by the the fact that at high energies the electrons jump into the higher valley where the electrons have a lower mobility than in the central Γ valley. The simulations suggest that the peak drift velocity for SiC is 2.2×10^5 ms^{-1}, while that for ZnO is $\sim 2 \times 10^5$ ms^{-1}. At higher electric fields, intervalley optical phonon emission dominates, causing the drift velocity to saturate at around 1.5×10^5 ms^{-1} for both structures. The threshold field for the onset of significant scattering into satellite conduction band valleys is a function of the intervalley separation and the density of electronic states in the satellite valleys. Comparison of our simulation results with experimental results measured by Khan

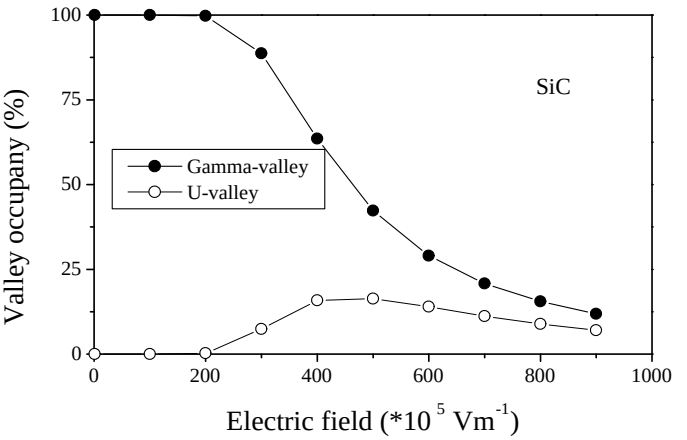

Fig. 4. Fractional occupation of the central Γ and satellite U valleys of SiC as a function of applied electric field using the non-parabolic band model at room temperature with $N_d = 10^{17}$ cm^{-3}.

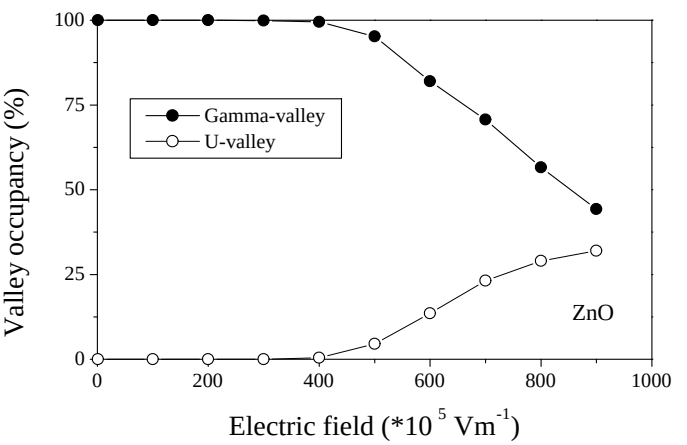

Fig. 5. Fractional occupation of the central Γ and satellite U valleys of ZnO as a function of applied electric field using the non-parabolic band model at room temperature with $N_d = 10^{17}$ cm^{-3}.

et al. for SiC in Fig. 1 shows a good agreement. From Figs. 4 and 5, which show the fractional occupancy of the available valleys as a function of applied field, the threshold fields are found to be 2×10^7 Vm^{-1} for SiC and 3.5×10^7 Vm^{-1} for the ZnO structure.

Also, from Fig. 6, it can be seen that intervalley transfer is substantially larger in the SiC than the ZnO structure, due to the combined effect of a lower Γ-valley effective mass, lower satellite valley separation and reduced phonon scattering rate within the Γ-valley, but significant intervalley phonon scattering at a threshold field of 2×10^7 Vm^{-1}.

Figures 6 and 7 show the calculated electron drift velocity in ZnO and SiC as a function of electric field strength for temperatures of 300, 450 and 600 K. The

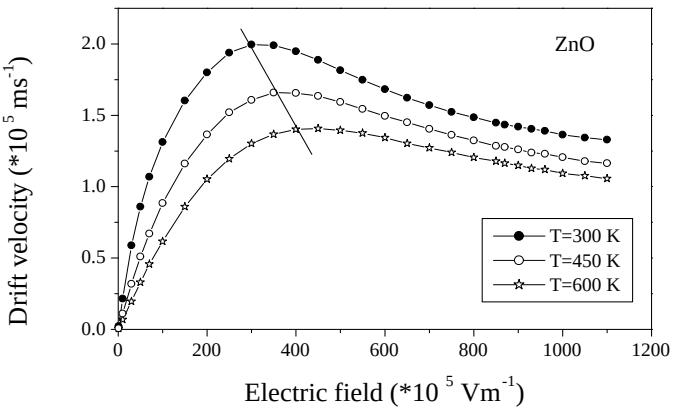

Fig. 6. Calculated electron steady state drift velocity in bulk ZnO as a function of applied electric field at various lattice temperatures and assuming a donor concentration of 10^{17}cm^{-3}. The peak drift velocity decreases by about 32% while the threshold field increases by same percentage as the lattice temperature increases from 300 to 600 K.

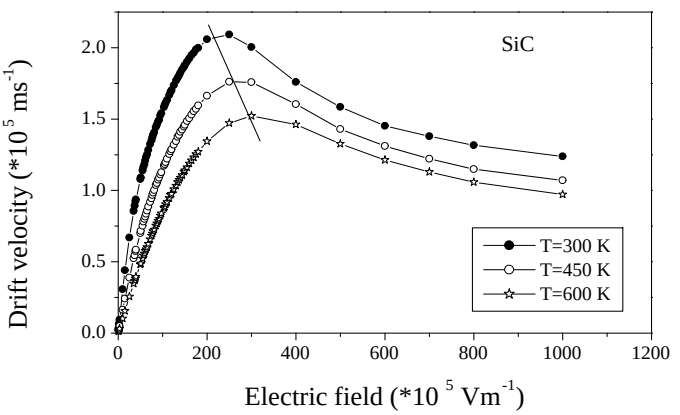

Fig. 7. Calculated electron steady state drift velocity in bulk SiC as a function of applied electric field at various lattice temperatures and assuming a donor concentration of 10^{17} cm^{-3}. The peak drift velocity decreases by about 25% while the threshold field increases by same percentage as the lattice temperature increases from 300 to 600 K.

decrease in drift mobility with temperature at low fields is due to increased intravalley polar optical phonon scattering whereas the decrease in velocity at higher fields is due to increased intra and intervalley scattering. It can be seen from the figures that the peak velocity also decreases and moves to higher electric field as the temperature is increased. This is due to the general increase of total scattering rate with temperature, which suppresses the electron energy and reduces the population of the satellite valleys. This latter effect is apparent from the fact that the electron population in the Γ-valley is higher in the ZnO material as shown in Fig. 8. Comparison of electron transport properties in wurtzite ZnO (Fig. 6) and

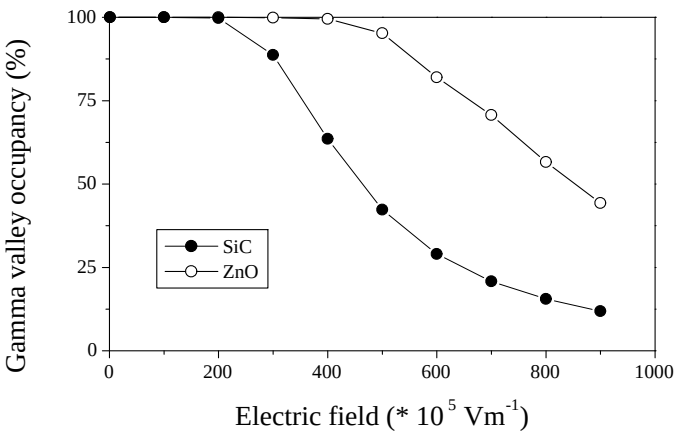

Fig. 8. Fraction of electrons in the Γ valley of ZnO and SiC materials as a function of applied electric field using the non-parabolic band model at room temperature with $N_d = 10^{17}$ cm^{-3}.

SiC (Fig. 7) shows that the change in peak velocity of ZnO from 300 K to 600 K is a reduction of about 32% whereas for SiC it is about 25%. Therefore, the electron velocity in SiC is less sensitive to temperature than in ZnO, and SiC devices are expected to be more tolerant to self-heating and high ambient temperature.

4. Conclusions

The calculated steady state electron transport in wurtzite SiC and ZnO materials using a hydrodynamic equation approach has been demonstrated. Our simulation results show that due to the high electron drift velocity in the two structures we can use these materials for device applications in high-power and high-temperature performance. The velocity-field characteristics of the materials show similar trends, reflecting the fact that these semiconductors have satellite valley effective densities of states several times greater than the central Γ-valley.

Acknowledgments

The authors gratefully acknowledge a grant from Ferdowsi University of Mashhad.

References

1. D. C. Look, D. C. Reynolds, J. R. Sizelove and W. C. Harsch, *Solid State Commun.* **105** (1998) 399.
2. P. Fons, K. Iwata, S. Niki, A. Yamada and K. Matsubara, *J. Cryst. Growth* **201** (1999) 627.
3. J. Narayan, K. Dovidenko, A. K. Sharma and S. Oktyabrskay, *J. Appl. Phys.* **84** (1998) 2597.
4. Y. Liu, C. R. Gorla, S. Liang, N. Emanetoglu and M. Wraback, *J. Electron Mater.* **29** (2000) 69.

5. B. Hahn, G. Heindel and W. Gebhardt, *Semicond. Sci. Tech.* **13** (1998) 788.
6. M. Kasuga and S. Ogawa, *Jpn. J. Appl. Phys.* **22** (1983) 794.
7. H. Arabshahi, *Mod. Phys. Lett. B* **20** (2006) 787.
8. H. Arabshahi and M. H. Ghasemian, *Mod. Phys. Lett. B* **22** (2006) 1397.
9. K. Tomizawa, *Numerical Simulation of Submicron Semiconductor Devices* (Artech House, London, Boston, 1993).
10. C. Jacoboni and P. Lugli, *Monte Carlo Method for Semiconductor and Device Simulation* (Springer-Verlag, 1989).
11. C. Moglestue, *Monte Carlo Simulation of Semiconductor Devices* (Chapman and Hall, 1993).
12. K. Blotekjaer, *IEEE Trans. Electron Dev.* **17** (1970) 38.
13. C. L. Gardner, *IEEE Trans. Electron Dev.* **38** (1991) 392.
14. Y. K. Feng and A. Hintz, *IEEE Trans. Electron Dev.* **35** (1988) 1419.
15. M. A. Alsunaidi, S. M. Hammadi and S. M. El-Ghazaly, *Int. J. Num. Mod.: Newt. Dev. Fields* **10** (1997) 107.
16. E. O. Kane, *J. Phys. Chem. Solids* **1** (1957) 249.
17. J. Kolnik, I. H. Oguzman and K. F. Brennan, *J. Appl. Phys.* **78** (1995) 1033.
18. B. E. Foutz, L. F. Eastman, U. V. Bhapkar and M. Shur, *Appl. Phys. Lett.* **70** (1997) 2849.
19. J. D. Albrecht, R. P. Wang, P. P. Ruden and K. F. Brennan, *J. Appl. Phys.* **83** (1998) 2185.
20. B. Gelmont, K. Kim and M. Shur, *J. Appl. Phys.* **74** (1993) 1818
21. J. W. Cooley and J. W. Tukey, *Math. Comput.* **19** (1965) 297.
22. G. D. Bergland, *Math. Comput.* **21** (1967) 236.
23. G. D. Bergland, *Math. Comput.* **22** (1968) 275.
24. C. Temperton, *J. Comput. Phys.* **34** (1980) 314.
25. M. Walmsley and R. A. Abram, *Int. J. Comput. Math.* **15** (1996) 31.
26. B. L. Buzbee, *SIAM J. Numer. Anal.* **18** (1999).
27. I. A. Khan and J. A. Cooper, *IEEE Trans. Electron Devices.* **47** (2000) 269.
28. I. A. Khan and J. A. Cooper, *Am. Sci. Forum* **264** (1998) 509.